AIP | Journal of Applied Physics

Resonant tunneling assisted propagation and amplification of plasmons in high electron mobility transistors

Shubhendu Bhardwaj, Berardi Sensale-Rodriguez, Huili Grace Xing, Siddharth Rajan, and John L. Volakis

Citation: Journal of Applied Physics **119**, 013102 (2016); doi: 10.1063/1.4939076
View online: http://dx.doi.org/10.1063/1.4939076
View Table of Contents: http://scitation.aip.org/content/aip/journal/jap/119/1?ver=pdfcov
Published by the AIP Publishing

Resonant tunneling assisted propagation and amplification of plasmons in high electron mobility transistors

Shubhendu Bhardwaj,[1] Berardi Sensale-Rodriguez,[2] Huili Grace Xing,[3,4] Siddharth Rajan,[5] and John L. Volakis
[1]*Electrical and Computer Engineering Department, The Ohio State University, Columbus, OH 43212*
[2]*Electrical and Computer Engineering Department, The University of Utah, Salt Lake City, UT 84112*
[3]*School of Electrical and Computer Engineering and Department of Materials Science and Engineering, Cornell University, Ithaca, NY 14853*
[4]*Department of Electrical Engineering, University of Notre Dame, IN 46556*
[5]*Electrical and Computer Engineering Department and Materials Science Engineering Department, The Ohio State University, Columbus, OH 43212*

(Received 16 November 2015; accepted 15 December 2015; published online 5 January 2016)

A rigorous theoretical and computational model is developed for the plasma-wave propagation in high electron mobility transistor structures with electron injection from a resonant tunneling diode at the gate. We discuss the conditions in which low-loss and sustainable plasmon modes can be supported in such structures. The developed analytical model is used to derive the dispersion relation for these plasmon-modes. A non-linear full-wave-hydrodynamic numerical solver is also developed using a finite difference time domain algorithm. The developed analytical solutions are validated via the numerical solution. We also verify previous observations that were based on a simplified transmission line model. It is shown that at high levels of negative differential conductance, plasmon amplification is indeed possible. The proposed rigorous models can enable accurate design and optimization of practical resonant tunnel diode-based plasma-wave devices for terahertz sources, mixers, and detectors, by allowing a precise representation of their coupling when integrated with other electromagnetic structures. © *2016 AIP Publishing LLC*.
[http://dx.doi.org/10.1063/1.4939076]

I. INTRODUCTION

Interest in terahertz technology has significantly risen in the past decade as an attractive alternative for a variety of sensing and telecommunication applications.[1,2] This has led to many terahertz applications. Among them, a critical need exists for terahertz sources, capable of operating at room-temperature with sufficient power for practical terahertz (THz) communication links. In this context, the conventional approach of decreasing gate-length can barely yield transistor operation beyond 1 THz.[3] Therefore, there is a need for alternate THz generation methods.[1,4,5] Among them, plasma-wave devices have offered a viable solution. This is because such devices operate by taking advantage of the electron-plasma oscillations in the 2 dimensional electron gas (2DEG) of high electron mobility transistors (HEMTs).

Notably, plasma-instability due to asymmetric boundary conditions at source and drain contacts of a short channel HEMT has been predicted to lead to self-sustained oscillations.[6–8] It is argued that, in such devices, the scattering losses in the channel are countered by amplification due to reflective boundary, leading to oscillations. Of importance is that the typical electron densities in the 2DEG of modern HEMT are in the range of 10^{12}–$10^{13}\,cm^{-2}$. Therefore, these oscillations have the potential to generate THz power. Indeed, experimental observations of these oscillations have been reported, often at cryogenic temperatures.[9–14] However, low loss electron plasma wave propagation at room-temperature as well as self-sustained oscillations in traditional semiconductor 2DEG structures are not yet practical. This is due to the limited electron mobility and large electron plasma wave damping at room-temperature in these materials.

To develop such plasma-wave THz devices at room-temperature, this low mobility limitations must be overcome by inserting additional gain mechanisms.[15–17] One of such approaches can be realized with the assistance of resonant tunnel diode (RTD) introduced at the gate and biased in the negative differential conductance region of its I-V characteristics.[18,19] RTDs operating beyond 1 THz have already been demonstrated.[20,21] In this paper, we show via analytical and numerical means that plasmons in RTD-gated HEMTs can indeed show amplification. Such a demonstration could indeed pave way to THz sources and amplifiers. Such RTD-gated devices could also serve as replacements for lossy dielectric waveguides in future terahertz integrated circuits.

In the following, we first derive the attenuation constants for propagating plasma-modes in a 2DEG channel of an RTD-gated HEMT. We find that appropriately large negative differential conductance (NDC) leads to negative attenuation constant, indicating growth of plasmonic oscillations. This analysis is next verified using full-wave simulations that model the Maxwell-Hydrodynamic equations. To that end, we also develop a finite difference time domain (FDTD) solver, already verified in Refs. 22–25, but here we also include the effect of the RTD-NDC. Finally, we discuss their relevance and show practical designs that can be realized for THz sources, amplifiers, and waveguide applications.

II. PLASMA PROPAGATION IN RTD-GATED 2DEG: SMALL SIGNAL ANALYSIS

Dispersion relations for propagating plasma waves such 2DEG channels are derived in the literature.[26–31] Specifically, Ref. 31 gives the attenuation due to finite mobility for a biased gated 2DEG layer. We will expand on the analysis to include the effect of RTD placed at the gate, adjacent to the 2DEG layer.

A schematic of the device under consideration is shown in Fig. 1. We consider a long, thin 2DEG channel under a metal gate separated by a vertical RTD at the barrier layer. The 2DEG channel is biased by applying source to drain voltage, while the RTD is biased using the gate's voltage with respect to the channels local potential. With this set-up, the current through the RTD is added to the 2DEG current. To simplify the analysis, and to be able to obtain closed form expression, we make following assumptions:

(1) RTD DC current is assumed to be small and does not cause significant variations in sheet-electron density or velocity along the channel. In other words, the DC conditions in the channel are dominated by drain to source bias (and not by the gate to channel bias).
(2) Variations in the RTD bias are small, allowing almost uniform NDC as we move along the channel.
(3) Plasma wavelength is much larger than barrier thickness d but is much smaller than the free-space wavelength.

With the above assumptions, we proceed to employ the electron transport equations in the channel. These are the first two moments of Boltzmann Transport Equation (BTE),[32] viz.,

$$\frac{\partial n_{sh}}{\partial t}+\frac{\partial j}{\partial x}=\left(\frac{\partial n_{sh}}{\partial t}\right)_{RTD}, \quad \text{and} \tag{1}$$

$$\frac{\partial j}{\partial t}+v\frac{\partial j}{\partial x}+j\frac{\partial v}{\partial x}=-\frac{qn_{sh}E_{ch}}{m_e}-\frac{j}{\tau}+v\left(\frac{\partial n_{sh}}{\partial t}\right)_{RTD}. \tag{2}$$

Here, n_{sh} is the sheet carrier density, $j=n_{sh}v$ is the sheet electron flux, and v is the electron velocity within the 2DEG channel. Also, E_{ch} is the x-directed electric field along the channel (see Fig. 1), τ refers to momentum relaxation time, m_e is the effective electron mass, and $q=1.6\times10^{-19}$ C is the charge of a single electron. To account for the small-signal current due to RTD, the term $(\frac{\partial n_{sh}}{\partial t})_{RTD}$ is added on the right hand side of (1). This term is much similar to generation recombination terms used in Ref. 33. Similarly, a change in the local momentum due to the RTD can be accounted for by introducing the term $v(\frac{\partial n_{sh}}{\partial t})_{RTD}$ in (2). This addition assumes that the electrons added due to the RTD quickly attain the local-bulk velocity in the channel, altering the momentum by $v(\frac{\partial n_{sh}}{\partial t})_{RTD}$. This is a reasonable assumption since electron tunneling is vertical to the 2DEG and electrons conserve momentum in the x-z plane. We note that (1) and (2) can be simplified by replacing $j=n_{sh}v$ in (2), giving

$$\frac{\partial n_{sh}}{\partial t}+\frac{\partial j}{\partial x}=\left(\frac{\partial n_{sh}}{\partial t}\right)_{RTD}, \quad \text{and} \tag{3}$$

$$\frac{\partial v}{\partial t}+v\frac{\partial v}{\partial x}=-\frac{qE_{ch}}{m_e}-\frac{v}{\tau}. \tag{4}$$

To derive the dispersion formulae from the above, our strategy is to first establish a relation between the channel AC current and the electric-field. This will provide an expression for the channel conductivity (σ_{ac}) in terms of $(\frac{\partial n_{sh}}{\partial t})_{RTD}$, which is related to the E-field profile in the barrier layer. Using this σ_{ac}, we can then employ the E and H-field boundary conditions to obtain the desired dispersion relations.

We proceed by introducing a small signal, space-time field perturbation, given by $E_{ch}=E_o+E_{ac}\exp(j\omega t-j\beta_x x)$. This leads to represent the electron density as $n_{sh}=n_o+n_{ac}\exp(j\omega t-j\beta_x x)$. Further, the associated velocity is given by $v=v_o+v_{ac}\exp(j\omega t-j\beta_x x)$. As can be seen, n_{ac} and v_{ac} are the amplitudes of the AC variations in the electron density and velocity, respectively. As expected, $\omega(=2\pi f)$ is the angular frequency and β_x is the propagation constant along the channel (i.e., in x-direction). We next introduce the known AC current representation

$$J_{ac} \quad =-qv_on_{ac}-qn_ov_{ac}-qn_{ac}v_{ac} \tag{5}$$

and by invoking (3) and (4), we get

$$J_{ac}=\frac{q^2E_{ac}}{m}\frac{(\partial n_{sh}/\partial t)_{RTD}+j\omega n_o}{\left(j\omega-j\beta_x v_o+\frac{1}{\tau}\right)(j\omega-j\beta_x v_o)} -\frac{qv_o(\partial n_{sh}/\partial t)_{RTD}}{j\omega-j\beta_x v_o}. \tag{6}$$

In the above, J_{ac} can be further simplified by introducing $(\frac{\partial n_{sh}}{\partial t})_{RTD}=\frac{-gV_{RTD}}{q}$, where V_{RTD} is the AC voltage is across the RTD barrier and g is the RTD differential conductance (in S/m^2). As expected, $V_{RTD}=-\int_{y=-d}^{y=0}E_y dy$ is related to the 2DEG field, E_{ac}. To derive this relation, we further consider the field profiles in the barrier layer $-d<y\le0$ and below the 2DEG layer $y\le-d$. Since we do not expect any E_z fields, we begin by introducing the vector potentials $\vec{F}=\hat{z}F_z$, where F_z is

$$F_z=\begin{cases}A\cos(\beta_y y)\exp(j\omega t-j\beta_x x); -d\le y\le0\\ B\exp(\alpha_y y)\exp(j\omega t-j\beta_x x); y<-d.\end{cases} \tag{7}$$

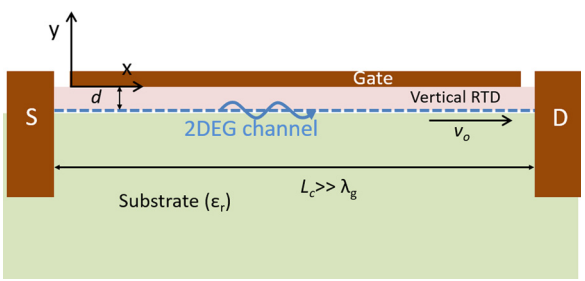

FIG. 1. Cross-sectional schematic of a HEMT with a vertical RTD between the gate and the channel. The dashed line represents the 2DEG and the S/D stand for source and drain.

Here, β_y is the propagation constant in the y-direction for the region $-d < y \leq 0$ and α_y is the attenuation constant for when $y \leq -d$. Further, by invoking the wave equation, we obtain the characteristic equations, $\beta_y^2 + \beta_x^2 = \beta^2$ and $-\alpha_y^2 + \beta_x^2 = \beta^2$ where $\beta = \omega\sqrt{\epsilon\mu_o}$ is the propagation constant of the wave in the dielectric. Here, we have $\epsilon = \epsilon_r\epsilon_o$, with ϵ_r being the dielectric constant. ϵ_o and μ_o are permittivity and permeability in the vacuum, respectively. In the above, A and B are to be eliminated via enforcement of the boundary conditions.

The field components corresponding to $\vec{F}$ are found from $\vec{E} = \frac{-1}{\epsilon}\nabla \times \vec{F}$, giving

$$E_x = \frac{-1}{\epsilon}\frac{\partial F_z}{\partial y} = \begin{cases} \frac{A\beta_y}{\epsilon}\sin(\beta_y y)\exp(j\omega t - j\beta_x x); -d \leq y \leq 0 \\ \frac{-B\alpha_y}{\epsilon}\exp(\alpha_y y)\exp(j\omega t - j\beta_x x);\ y < -d, \end{cases} \tag{8}$$

$$E_y = \frac{1}{\epsilon}\frac{\partial F_z}{\partial x} = \begin{cases} \frac{-Aj\beta_x}{\epsilon}\cos(\beta_y y)\exp(j\omega t - j\beta_x x); -d \leq y \leq 0 \\ \frac{-B\beta_x}{\epsilon}\exp(\alpha_y y)\exp(j\omega t - j\beta_x x);\ y < -d, \end{cases} \tag{9}$$

also, $H_z = -j\frac{1}{\omega\mu\epsilon}\left(\frac{\partial^2}{\partial z^2} + \beta^2\right)F_z$, viz.,

$$H_z = \frac{-j\beta^2 F_z}{\omega\mu\epsilon} = \begin{cases} \frac{-j}{\omega\mu\epsilon}\beta^2 A\cos(\beta_y y)\exp(j\omega t - j\beta_x x); -d \leq y \leq 0 \\ \frac{-j}{\omega\mu\epsilon}\beta^2 B\exp(\alpha_y y)\exp(j\omega t - j\beta_x x);\ y < -d. \end{cases} \tag{10}$$

Recognizing that the channel-field E_{ac} can be obtained by $E_{ac} = E_x^{y=-d}$, and then dividing E_{ac} by (9) gives E_y in terms of E_{ac}

$$E_y = \frac{j\beta_x E_{ac}}{\beta_y \sin(\beta_y d)}\cos(\beta_y y). \tag{11}$$

Also, from

$$V_{RTD} = -\int_{y=-d}^{y=0} E_y dy = -\frac{j\beta_x E_{ac}}{\beta_y^2}, \tag{12}$$

we get

$$\left(\frac{\partial n_{sh}}{\partial t}\right)_{RTD} = -\frac{gV_{RTD}}{q} = g\frac{j\beta_x E_{ac}}{q\beta_y^2}. \tag{13}$$

Above can is used to replace the term $\left(\frac{\partial n_{sh}}{\partial t}\right)_{RTD}$ in (6). After further algebraic manipulations, (6) becomes

$$J_{ac} = \sigma_{ac}E_{ac} + \gamma E_{ac}^2, \tag{14}$$

where

$$\sigma_{ac} = \frac{q^2}{m_e}\frac{j\omega n_o}{(j\omega - j\beta_x v_o)(j\omega - j\beta_x v_o + 1/\tau)} - \frac{v_o\beta_x g}{\beta_y^2(\omega - v_o\beta_x)},$$

and

$$\gamma = \frac{q^2}{m_e(j\omega - j\beta_x v_o)(j\omega - j\beta_x v_o + 1/\tau)} \times \left[\frac{-jq\beta_x n_o}{m(j\omega - \beta_x v_o + 1/\tau)} - \frac{j\beta_x g}{q\beta_y^2}\right].$$

Since E_{ac}^2 is small, an additional simplification is to ignore the E_{ac}^2 term. Doing so, we obtain a linear current-field relation for determining the channel AC conductivity σ_{ac}. An expression for channel-conductivity was derived in Ref. 31 as well, but (14) above also accounts for the effect of NDC g, as controlled by the second term of σ_{ac}.

We next proceed to enforce the other boundary conditions and therefore eliminate the A and B constants. Specifically, we have $H_z|_{y=-d^+} - H_z|_{y=-d^-} = \sigma_{ac}E_x|_{y=-d}$ long with $E_x|_{y=-d^+} = E_x|_{y=-d^-}$. When these are substituted in (8)–(10), we get

$$\cot(\beta_y d) \pm j = \frac{\sigma_{ac}\beta_y}{j\omega\epsilon}, \tag{15}$$

with σ_{ac} as given in (14). This can be simplified to a quadratic equation in β_y, using $\cot\beta_y d \approx \frac{1}{\beta_y d}$ since the barrier thickness d is much smaller than the plasma-wavelength and $\beta_x \gg \beta$. Thus, we have

$$\beta_x^2\left(-v_o^2 + \frac{q^2 n_o d}{m_e\epsilon} - \frac{jgdv_o^2}{\omega\epsilon}\right) + \beta_x\left(2v_o\omega - \frac{jv_o}{\tau} + \frac{jv_o gd}{\epsilon} + \frac{v_o gd}{\omega\tau\epsilon}\right) + \frac{j\omega}{\tau} - \omega^2 = 0. \tag{16}$$

This new relation allows us to find the plasma-wave propagation constant as a function of ω, while considering the effect of NDC g. We note that for $g = 0$, (16) converges to the dispersion relation for the plasma-wave propagation in the gated 2-DEG as derived in Ref. 31. This serves as verification for above calculations.

Dispersion curves can be obtained by solving the quadratic equation (16). The two solutions to (16) correspond to wave moving in forward and backward directions. Here, we define forward wave as that traveling in the direction of the electron drift velocity due to drain to source bias, i.e., $\Re(\beta_x) > 0$ for $v_o > 0$. Hereon, we only consider the forward wave, since the backward wave is associated with much higher attenuation and is not of interest (as also reported in Refs. 22 and 31).

A. Solution for RTD-gated GaN/AlGaN heterojunction

As a next step, we evaluated the developed solution for a GaN/AlGaN heterojunction with an RTD placed at the gate.

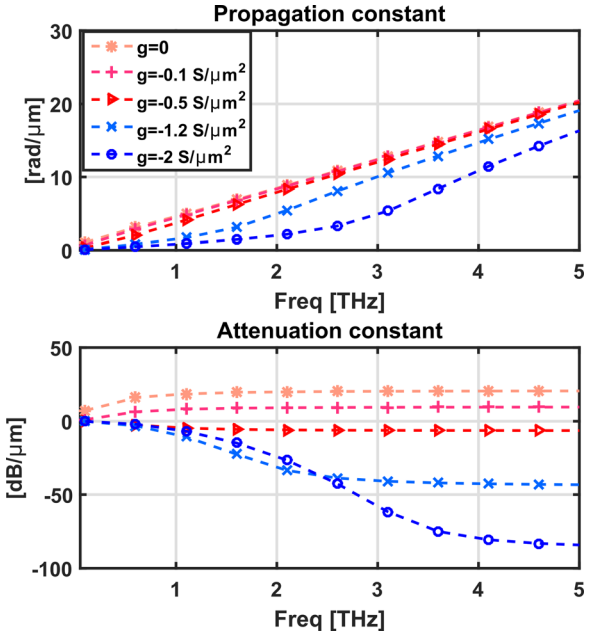

FIG. 2. Propagation constant and attenuation of the plasma waves as a function of changing differential conductivity g of the RTD. For calculations, we considered $\tau = 0.1366$ ps, $v_o = 10^7$ cm/s $\epsilon_r = 9.5$ for GaN, $n_o = 5 \times 10^{12}$ cm^{-2}, and $d = 25$ nm. (Negative values signify wave amplification.)

For the given material system, parameters chosen are $\epsilon_r = 9.5$, $n_o = 5 \times 10^{12}$ cm^{-2}, $d = 25$ nm, $\tau = 0.1366$ ps, and $v_o = 10^7$ cm/s. Fig. 2 shows the effect of RTD differential conductance g on the wave propagation. Specifically, the phase constant ($\Re(\beta_x)$) and attenuation constant α ($= -\Im(\beta_x)$) are plotted as a function of frequency. We observe that increasing the value $-g$ gradually decreases the attenuation constant, eventually causing amplification. From these plots, we can conclude a $g < -0.5\, S/\mu m^2$ is needed for plasma-wave amplification. However, since plasma-wave losses are higher for smaller relaxation time, τ, the attenuation constant is expected to increase accordingly.

Fig. 3 shows the attenuation constants at frequencies 1 THz and 5 THz as a function of τ and g. As expected, the wave amplification is highest for large τ and large $-g$. We also note that NDC needed for amplification becomes smaller, when τ is large (refer to the $\alpha = 0$ contour).

The above analysis suggests that the RTD-gate can reinforce plasma-wave propagation, reducing losses and even causing amplification in accordance with the NDC value provided by the RTD. To further validate the analysis, we consider comparisons with the full-wave hydrodynamic simulations. These comparisons are presented next.

III. FULL-WAVE MODELING OF RTD-GATED HEMT: VALIDATION AND RESULTS

In this section, we validate the aforementioned analysis using numerical FDTD simulations. Indeed, FDTD simulations have already been used for numerical modeling of plasma-waves for a 2DEG layer embedded in a dielectric media.[22,25] Using the same algorithm, we recently developed models for plasma-waves in confined 2DEGs.[23,24] In this work, we expand on this model to consider the presence of an

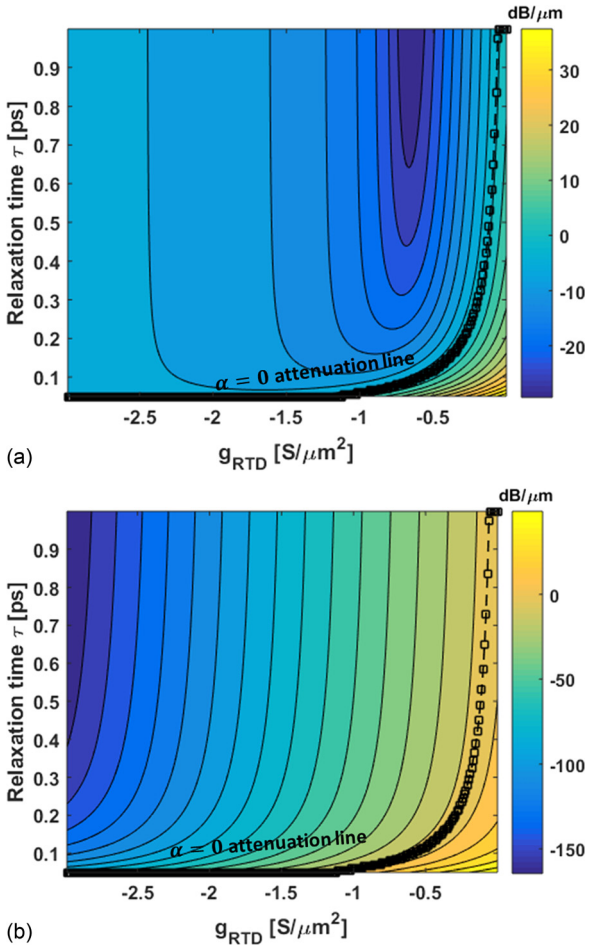

FIG. 3. Attenuation constant as a function of relaxation time (τ) and RTD-NDR (g). The marked line refers to the zero attenuation contour. For the calculations, we considered $v_o = 10^7$ cm/s, $\epsilon_r = 9.5$ for GaN, $n_o = 5 \times 10^{12}$cm^{-2}, and $d = 25$ nm. (a) Plots at frequency $f = 1$ THz. (b) Plots at frequency $f = 5$ THz. (Negative values signify wave amplification.)

RTD-NDC between the 2DEG channel and the gate. Below, we briefly discuss the developed numerical model and then use it to calculate dispersion relations. These will be compared with the analytical model given in Sec. II.

A. Full-wave-hydrodynamic FDTD analysis for RTD-gated HEMT

As discussed in Sec. II, the electron-transport properties of the channel are modeled using the mass and momentum conservation equations (1) and (2). These are modified with added terms to account for the presence of RTD AC current. To model the electromagnetic fields in the vicinity of this channel, we also considered Maxwell's equations

$$\nabla \times \vec{H} = \frac{\partial \vec{D}}{\partial t} + \vec{J}, \quad \text{and} \tag{17}$$

$$\nabla \times \vec{E} = -\frac{\partial \vec{B}}{\partial t}. \tag{18}$$

In the above, symbols carry their usual meaning. The current density excitation $\vec{J}$ is provided from the hydrodynamic sheet current and is given by

$$\vec{J} = \frac{-q(j - j_o)}{t_{2DEG}}\hat{x}, \tag{19}$$

where t_{2DEG} is the modeled thickness of the 2DEG layer, $j_o = n_o v_o$ is initial DC sheet current, and $j = nv$ is total sheet current. Specifically, $j - j_o$ represents the AC sheet current responsible for electromagnetic radiation from the channel.

We applied the 2D-FDTD algorithm[34] to solve equations (3), (4), and (17)–(19) for the device cross-section, as shown in Fig. 1. Specifically, Maxwell's equations were replaced by their corresponding time and space difference equations. Likewise, HD equations were discretized using 1D model since thickness, t_{2DEG}, was assumed to be of single grid size, chosen to be 2.5 nm. It is important to note that due to non-linear and coupled nature of HD equations, center differencing approach was not used. Rather, the upwind differencing scheme was applied for stability. At the channel boundaries, we assume charge neutral contacts, i.e., $n_{sh}(x = 0) = n_{sh}(x = L_c) = n_o$. For the Maxwell's equations, we modeled these contacts as perfect electrical conductors (PEC). Thus, field-reflection and diffraction near them are accounted for. Similar to ohmic-contacts, the metal gate was also modeled with the PEC boundary condition.

FDTD algorithm was employed to solve the Maxwell's and HD equations in-tandem. That is, in each time step, the fields and currents were updated via Maxwell and HD solvers, respectively. To couple the two solvers, the updated channel fields from the Maxwell solver were used as excitation terms in HD solver. Subsequently, the updated current from HD solver provided the source term to the Maxwell solver. Using this scheme, self-consistency was achieved among these equations.

B. Comparison of numerical and analytical solutions

As already noted, the derivation of the dispersion relation (16), assumes linearization of the hydrodynamic equations. Specifically, second order variations (v_{ac}^2, n_{ac}^2, etc.) are ignored, as noted in (14). Additionally, we also assume that $\beta_y d \ll 1$ and $\beta_x^2 \approx -\beta_y^2 \gg \beta^2$. These assumptions were needed to obtain a closed form solution. Therefore, to validate the analytical results using full-wave simulations, we must carefully choose the frequency band and the parameters where these approximations hold true. For the comparison, we chose parameters typical to a 2DEG channel in GaN/AlGaN heterojunctions, except for its dielectric constant. We chose $\epsilon_r = 1$, so that approximation $\beta_y d \ll 1$ is valid due to larger plasma-wavelength for smaller ϵ_r. Other parameters used were $n_o = 5 \times 10^{12}\,\text{cm}^{-2}$, $\tau = 0.137\,\text{ps}$, $v_o = 10^7\,\text{cm/s}$, and $m_e = 0.2m_o$. We chose the thickness of the 2DEG layer to be $t_{2DEG} = 2.5\,\text{nm}$.

To obtain the dispersion curve, we need to excite a broadband THz plasma-wave in 2DEG and then record its propagation and attenuation constant as it travels along the channel. To do so, we model a THz pulse incident on the HEMT which contains a long and RTD-gated channel ($L_c = 10\,\mu\text{m}$), having a small gap-discontinuity at the gate. This model is shown in Fig. 4. The incident wave diffracts through the gap and couples with the channel to excite the propagating plasmonic modes. We record the time domain signal at different points in the channel and extract the attenuation and phase constants by Fourier transformation across the band of interest. The results are plotted in Fig. 5.

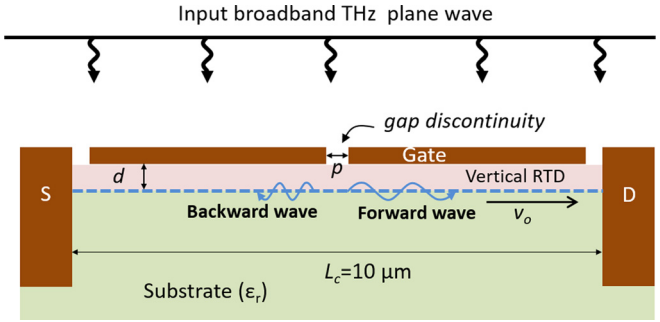

FIG. 4. Model used for the numerical calculations. The size of the discontinuity is chosen to be $p = 40\,\text{nm}$.

As seen, there is good agreement between the wavenumbers obtained from the two models. Notably, both models predict only a negligible change in the wavenumber with varying g. These plots also demonstrate an agreement in the attenuation constants calculated via the two models. Here, we also confirm that the attenuation constant decreases with the increasing $-g$. Small variations in the simulated results were observed due to the inherent non-linearity of the numerical solver and reflection from source and drain terminals.

Next, a similar comparison is made for a practical case of GaN/AlGaN device, where dielectric constant is set $\epsilon_r = 9.5$. The comparisons are shown in Fig. 6. We again confirm the reduction of the attenuation constant as predicted

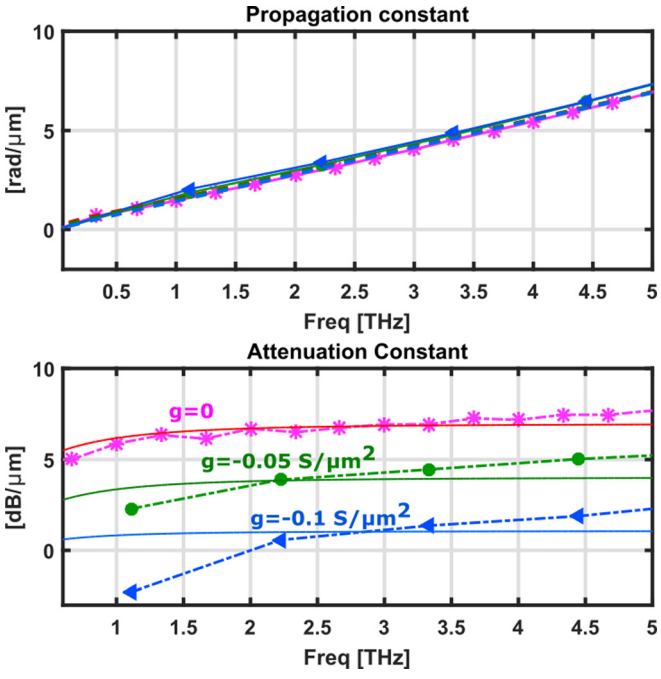

FIG. 5. Wavenumbers and the attenuation constants obtained using the full-wave method and the analytical method in Sec. II. The "symbol" lines refer to numerical simulations and the solid lines refer to the analytical model. Choice of parameters: $\epsilon_r = 1$, $d = 25\,\text{nm}$, $n_o = 5 \times 10^{12}\,\text{cm}^{-2}$, $\tau = 0.137\,\text{ps}$, $v_o = 10^7\,\text{cm/s}$, and $m_e = 0.2m_o$.

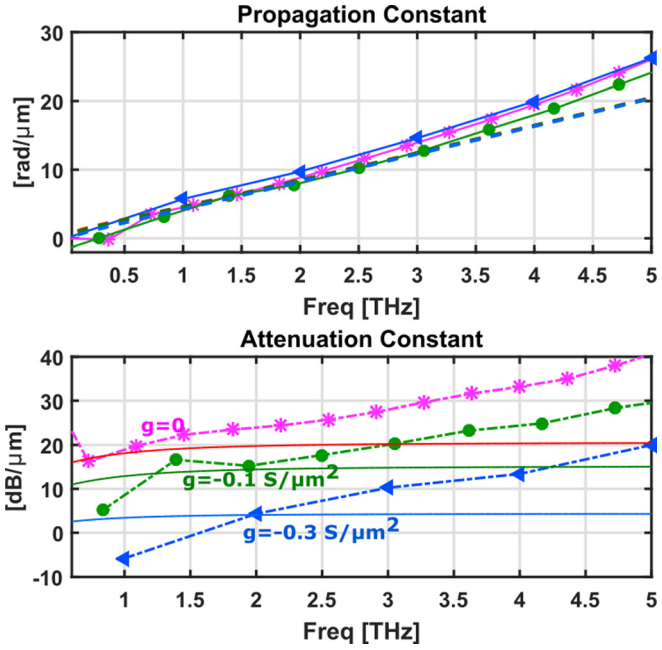

FIG. 6. Wavenumbers and the attenuation constants for GaN based RTD-gated HEMT obtained using the full-wave method and the analytical method in Sec. II. The "symbol" lines refer to numerical simulations, and the solid lines refer to the analytical model. Choice of parameters: $\epsilon_r = 9.5$, $d = 25$ nm, $n_o = 5 \times 10^{12}$ cm^{-2}, $\tau = 0.137$ ps, $v_o = 10^7$ cm/s, and $m_e = 0.2m_o$.

by the analytical model. Notably, more deviations are observed between the two models specially at larger frequencies. This is due to the higher dielectric constant causing $\beta_y d$ to become large, violating the assumptions made in the analysis. For example, at 3 THz $\beta_y d$ is close to 0.3.

From above, we infer that the analytical model correctly captures the phenomenon in the regime of long plasma-wavelengths. On the other hand, the full-wave-hydrodynamic model provides rigorous and accurate solution for all frequencies. It is also noted that for $\epsilon_r > 1$, analytical solution deviates from full-wave simulations. In such cases, use of full-wave-hydrodynamic simulations is recommended for design while the analytical model can be used for initial estimates.

IV. PLASMON PROPAGATION IN RTD-GATED GaN/AlGaN HETEROJUNCTIONS

In this section, we employ numerical solution to show the field-visualization for intuitive understanding of the proposed concept. The model and the excitation method are the same as in Sec. III, but now we chose excitation frequency of 5 THz. All other parameters are set as $n_o = 5 \times 10^{12}$ cm^{-2}, $\tau = 0.137$ ps, $v_o = 10^7$ cm/s, $\epsilon_r = 9.5$, and $m_e = 0.2m_o$.

Fig. 7 shows the coupling and propagation of plasma-waves for varying values of RTD-NDC. For $g = -0.5\,S/\mu m^2$, plasmon attenuation is reduced allowing propagation to longer distances. This observation is very useful for active terahertz waveguides. For the case of large NDC ($g = -0.8\ S/\mu m^2$ and $-1\,S/\mu m^2$), a growing propagating plasma-wave was also observed. With appropriate antennas at the input (source-gate) and output (drain-gate) terminals, an antenna-coupled amplifier

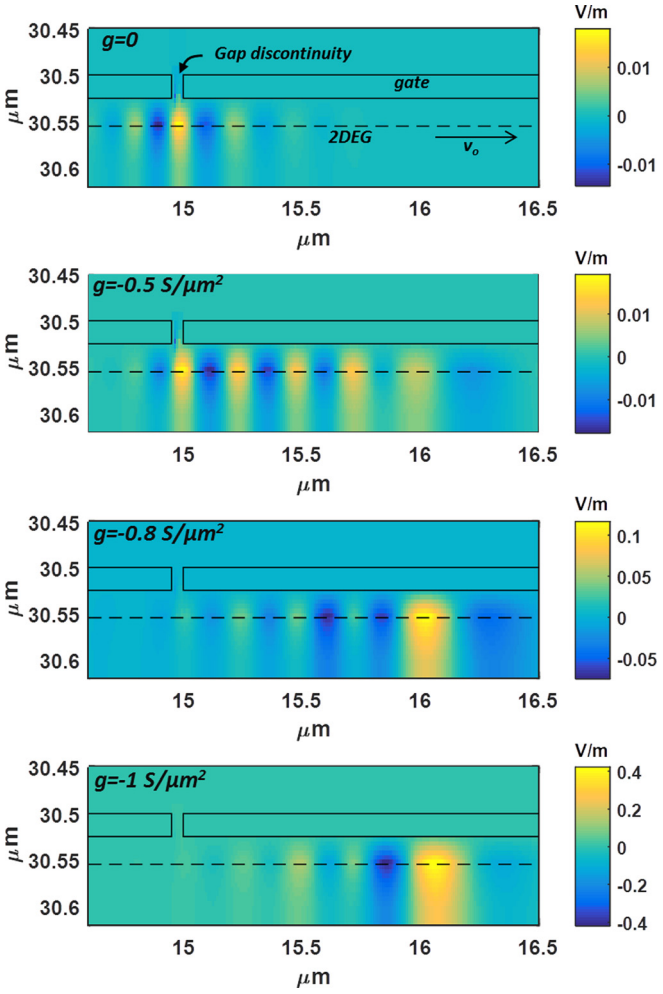

FIG. 7. E_x field snapshots taken at $t = 2$ ps. Detail along the partial section of the channel. Plasma-wave propagation for varying values of the RTD-NDC g is shown. Reduced plasma-wave losses and amplification can be obtained with increasingly $-g$. (Note: x and y axis are drawn with respect to the corner of the 2D-simulation domain and figure shows the zoomed in view.)

configuration can be achieved.[19] Clearly, this would require impedance-matching of the input and output terminals with the corresponding radiating structures. If left unmatched, the amplified plasma-wave would simply be reflected back from the drain terminal. This backward traveling wave would quickly attenuate due to opposite flow of electrons and large $-g$. Another way of achieving input-output coupling in the amplifier mode could be by using grating-gates.[25]

The shown concept can also be utilized to obtain a terahertz source.[23] As stated, the RTD-gate provides the much needed gain media for the propagating plasmons. Alongside this gain-media, a resonance mechanism is also needed to complete the oscillator action. This resonance is obtained by having periodic grating-gates instead of a single continuous gate. As predicted in Ref. 23, an RTD-gated, grating gate HEMT is expected to emit terahertz radiations. Of course, the frequency of resonance would be decided by the grating periodicity, 2DEG electron density, and barrier thickness. Note that, in such devices, the grating-gate also provides the needed coupling for the effective radiation of the terahertz plasmons.

V. CONCLUSION

We demonstrated that RTD-gated HEMTs support low-attenuation and growing plasma modes within the 2DEG channel. Depending on the value of the RTD-NDC, either a long distance plasma-wave propagation or amplification action can be sustained within the gated channel. This mode enhancement is supported by the RTD-gain mechanism, which counters the scattering losses in the channel. Our full-wave-hydrodynamic model and analytical expressions are validated for this concept.

We also concluded that, in practice, such devices would depend on fabrication of the state-of-the-art RTDs, operating at THz frequencies. Such RTDs are already being reported.[20,21] The NDC values available in these RTDs are of the order of 10 $mS/\mu m^2$. Although these values are smaller than the required, development of low-loss active THz-waveguides is possible using these RTDs. For THz-sources and amplifiers, higher NDC values would be required, which could allow these applications in future.

ACKNOWLEDGMENTS

This work was supported by the Office of Naval Research DATE MURI (Devices and Architectures for Terahertz Electronics Multi-university Research Initiative), under Grant No. N00014-11-1-0721.

[1]J. Ward, E. Schlecht, G. Chattopadhyay, A. Maestrini, J. Gill, F. Maiwald, H. Javadi, and I. Mehdi, "Capability of THz sources based on Schottky diode frequency multiplier chains," in *IEEE MTT-S International Microwave Symposium Digest* (2004), Vol. 3, pp. 1587–1590.
[2]R. Piesiewicz, T. Kleine-Ostmann, N. Krumbholz, D. Mittleman, M. Koch, J. Schoebel, and T. Kurner, "Short-range ultra-broadband terahertz communications: Concepts and perspectives," IEEE Antennas Propag. Mag. **49**, 24–39 (2007).
[3]B. Song, B. Sensale-Rodriguez, R. Wang, J. Guo, Z. Hu, Y. Yue, F. Faria, M. Schuette, A. Ketterson, E. Beam, P. Saunier, X. Gao, S. Guo, P. Fay, D. Jena, and H. Xing, "Effect of fringing capacitances on the RF performance of GaN HEMTs with T-gates," IEEE Trans. Electron Devices **61**, 747–754 (2014).
[4]B. S. Williams, "Terahertz quantum-cascade lasers," Nat. Photonics **1**, 517–525 (2007).
[5]E. R. Brown, K. A. McIntosh, K. B. Nichols, and C. L. Dennis, "Photomixing up to 3.8 THz in low-temperature-grown GaAs," Appl. Phys. Lett. **66**, 285–287 (1995).
[6]M. Dyakonov and M. Shur, "Shallow water analogy for a ballistic field effect transistor: New mechanism of plasma wave generation by dc current," Phys. Rev. Lett. **71**, 2465–2468 (1993).
[7]M. Dyakonov and M. Shur, "Detection, mixing, and frequency multiplication of terahertz radiation by two-dimensional electronic fluid," IEEE Trans. Electron Devices **43**, 380–387 (1996).
[8]M. Dyakonov and M. S. Shur, "Current instability and plasma waves generation in ungated two-dimensional electron layers," Appl. Phys. Lett. **87**, 111501 (2005).
[9]W. Knap, Y. Deng, S. Rumyantsev, and M. S. Shur, "Resonant detection of subterahertz and terahertz radiation by plasma waves in submicron field-effect transistors," Appl. Phys. Lett. **81**, 4637–4639 (2002).
[10]A. El Fatimy, F. Teppe, N. Dyakonova, W. Knap, D. Seliuta, G. Valuis, A. Shchepetov, Y. Roelens, S. Bollaert, A. Cappy, and S. Rumyantsev, "Resonant and voltage-tunable terahertz detection in InGaAs/InP nanometer transistors," Appl. Phys. Lett. **89**, 131926 (2006).
[11]X. G. Peralta, S. J. Allen, M. C. Wanke, N. E. Harff, J. A. Simmons, M. P. Lilly, J. L. Reno, P. J. Burke, and J. P. Eisenstein, "Terahertz photoconductivity and plasmon modes in double-quantum-well field-effect transistors," Appl. Phys. Lett. **81**, 1627 (2002).
[12]W. Knap, J. Lusakowski, T. Parenty, S. Bollaert, A. Cappy, V. V. Popov, and M. S. Shur, "Terahertz emission by plasma waves in 60 nm gate high electron mobility transistors," Appl. Phys. Lett. **84**, 2331–2333 (2004).
[13]J. Lusakowski, W. Knap, N. Dyakonova, L. Varani, J. Mateos, T. Gonzalez, Y. Roelens, S. Bollaert, A. Cappy, and K. Karpierz, "Voltage tuneable terahertz emission from a ballistic nanometer InGaAs/InAlAs transistor," J. Appl. Phys. **97**, 064307 (2005).
[14]M. Vosseburger, H. Roskos, F. Wolter, C. Waschke, H. Kurz, K. Hirakawa, L. Wilke, and K. Yamanaka, "Emission of THz radiation from optically excited coherent plasmons in a two-dimensional electron gas," *Summaries of Papers Presented in Quantum Electronics and Laser Science Conference, QELS'96* (1996), pp. 206–207.
[15]V. Ryzhii, M. Ryzhii, A. Satou, N. Ryabova, T. Otsuji, V. Mitin, F. T. Vasko, A. A. Dubinov, V. Y. Aleshkin, and M. S. Shur, "Graphene-based terahertz devices: Concepts and characteristics," in *Future Trends in Microelectronics* (John Wiley and Sons, Inc., 2010), pp. 293–306.
[16]F. Rana, "Graphene terahertz plasmon oscillators," IEEE Trans. Nanotechnol. **7**, 91–99 (2008).
[17]T. Otsuji, V. Popov, and V. Ryzhii, "Active graphene plasmonics for terahertz device applications," J. Phys. D: Appl. Phys. **47**, 094006 (2014).
[18]B. Sensale-Rodriguez, P. Fay, L. Liu, D. Jena, and H. Xing, "Enhanced terahertz detection in resonant tunnel diode-gated HEMTs," ECS Trans. **49**, 93–102 (2012).
[19]B. Sensale-Rodriguez, L. Liu, P. Fay, D. Jena, and H. Xing, "Power amplification at THz via plasma wave excitation in RTD-gated HEMTs," IEEE Trans. Terahertz Sci. Technol. **3**, 200–206 (2013).
[20]M. Asada, S. Suzuki, and N. Kishimoto, "Resonant tunneling diodes for sub-terahertz and terahertz oscillators," Jpn. J. Appl. Phys., Part 1 **47**, 4375 (2008).
[21]Y. Koyama, R. Sekiguchi, and T. Ouchi, "Oscillations up to 1.40 THz from resonant-tunneling-diode-based oscillators with integrated patch antennas," Appl. Phys. Express **6**, 064102 (2013).
[22]M. Khorrami, S. El-Ghazaly, H. Naseem, and S.-Q. Yu, "Global modeling of active terahertz plasmonic devices," IEEE Trans. Terahertz Sci. Technol. **4**, 101–109 (2014).
[23]S. Bhardwaj, B. Sensale-Rodriguez, H. Xing, and J. L. Volakis, "Full-wave hydrodynamic model for predicting thz emission from grating-gate rtd-gated plasma wave hemts," in 73rd Device Research Conference (2015).
[24]S. Bhardwaj, S. Rajan, and J. Volakis, "Room temperature detection of plasma resonances using multiple 2DEG channels in HEMT," in IEEE International Symposium on Antennas and Propagation (APSURSI-2015), Vancouver (2015).
[25]T. Otsuji, M. Hanabe, T. Nishimura, and E. Sano, "A grating-bicoupled plasma-wave photomixer with resonant-cavity enhanced structure," Opt. Express **14**, 4815–4825 (2006).
[26]F. Stern, "Polarizability of a two-dimensional electron gas," Phys. Rev. Lett. **18**, 546–548 (1967).
[27]M. Nakayama, "Theory of surface waves coupled to surface carriers," J. Phys. Soc. Jpn. **36**, 393–398 (1974).
[28]A. Eguiluz, T. K. Lee, J. J. Quinn, and K. W. Chiu, "Interface excitations in metal-insulator-semiconductor structures," Phys. Rev. B **11**, 4989–4993 (1975).
[29]L. Zheng, W. L. Schaich, and A. H. MacDonald, "Theory of two-dimensional grating couplers," Phys. Rev. B **41**, 8493–8499 (1990).
[30]S. J. Allen, D. C. Tsui, and R. A. Logan, "Observation of the two-dimensional plasmon in silicon inversion layers," Phys. Rev. Lett. **38**, 980–983 (1977).
[31]M. Ali Khorrami, S. El-Ghazaly, S.-Q. Yu, and H. Naseem, "Terahertz plasmon amplification using two-dimensional electron-gas layers," J. Appl. Phys. **111**, 094501 (2012).
[32]D. Vasileska, G. Klimeck, and S. M. Goodnick, *Computational Electronics, Semiclassical and Uqantum Device Modeling and Simulation* (CRC Press, 2010).
[33]K. Blotekjaer, "Transport equations for electrons in two-valley semiconductors," IEEE Trans. Electron Devices **17**, 38–47 (1970).
[34]A. Taflove and S. C. Hagness, *Computational Electrodynamics, The finite Difference Time Domain Method* (Artech House, Norwood, USA, 2005).